Ultramicroscopy 231 (2021) 113299

Contents lists available at ScienceDirect

Ultramicroscopy

journal homepage: www.elsevier.com/locate/ultramic

Detecting minute amounts of nitrogen in GaNAs thin films using STEM and CBED

Maryam Vatanparast [a], Yu-Tsun Shao [b], Mohana Rajpalke [c], Bjørn-Ove Fimland [c], Turid Reenaas [a], Randi Holmestad [a,*], Per Erik Vullum [a,d], Jian Min Zuo [a,e]

[a] Department of Physics, Norwegian University of Science and Technology (NTNU), NO-7491 Trondheim, Norway
[b] Department of Materials Science and Engineering, University of Illinois at Urbana-Champaign, Urbana, IL 61801, USA
[c] Department of Electronic Systems, NTNU, NO-7491 Trondheim, Norway
[d] SINTEF Industry, Richard Birkelands vei 2B, NO-7491 Trondheim, Norway
[e] Materials Research Laboratory, University of Illinois at Urbana-Champaign, Urbana, IL 61801, USA

ARTICLE INFO

Keywords:
Convergent beam electron diffraction (CBED)
Gallium arsenide (GaAs)
Scanning transmission electron microscopy (STEM)

ABSTRACT

Nitrogen (N) is a common element added to GaAs for band gap engineering and strain compensation. However, detection of small amounts of N is difficult for electron microscopy as well as for other chemical analysis techniques. In this work, N in GaAs is examined by using different transmission electron microscopy (TEM) techniques. While both dark-field TEM imaging using the composition sensitive (002) reflections and selected area diffraction reveal a significant difference between the doped thin-film and the GaAs substrate, spectroscopy techniques such as electron energy loss and energy dispersive X-ray spectroscopy are not able to detect N. To quantify the N content, quantitative convergent beam electron diffraction (QCBED) is used, which gives a direct evidence of N substitution and As vacancies. The measurements are enabled by the electron energy-filtered scanning CBED technique. These results demonstrate a sensitive method for composition analysis based on quantitative electron diffraction.

1. Introduction

The promise of the III-V compounds added with small amounts of nitrogen (N) is based on the possibility to tailor optical and electrical properties through composition-based energy bandgap engineering [1]. In particular, the III-V semiconductor compound GaAs with N added for the formation of dilute GaN_xAs_{1-x} alloys ($x \sim 0.01 - 0.06$) has attracted large interest in the past two decades. This is because of its unique properties and potential applications in novel optoelectronic devices, especially in high efficiency multi-junction solar cells [2,3], photodetectors [4,5] and infrared lasers [6]. The promise of the III-V-N compounds is based on the possibility to tailor optical and electrical properties through composition-based energy bandgap engineering [6]. Substitution of As by N drastically reduces the bandgap energy in GaAs [7]. In addition, the cubic lattice parameter decreases as a function of increasing N concentration. For this reason, GaNAs is also used for strain compensation in device structures [8]. A major challenge in the III-V-N dilute nitride-based devices, regardless of the use of modern epitaxial growth techniques, is poor material quality. N incorporation is often accompanied with an increase in structural defects, which degrade the device performances [9–11]. Questions have also been raised on how N is incorporated into the crystal lattice, whether it is substitutional or interstitial. Therefore, an accurate determination of the N concentration and its incorporation mechanism in III-V-N is necessary to further develop these dilute semiconductor compounds.

The detection of minority atoms in general is challenging for materials characterization. Transmission electron microscopy (TEM) with its high spatial resolution, is a powerful tool. Various TEM based approaches have been developed for composition characterization at the atomic level. For example, a small amount of carbon (C) in steel can be detected down to a threshold concentration using electron energy loss spectroscopy (EELS). Using a theoretical model, Natusch et al. concluded that the detection limit of C in steel was not better than 1.9 at. % C, given the instrumentation available at the time of publication [12]. Another approach is based on the measurement of strain and the use of Vegard's law for local composition determination. For example, the

Paper submitted in honor of Professor John Spence on his 75 years anniversary.

* Corresponding author.
E-mail address: randi.holmestad@ntnu.no (R. Holmestad).

https://doi.org/10.1016/j.ultramic.2021.113299
Received 22 December 2020; Received in revised form 12 April 2021; Accepted 24 April 2021
Available online 7 May 2021

concentration of N in the GaN_xAs_{1-x} quantum wells ($0.01 \leq x \leq 0.05$) was determined from high-angle annular dark-field (HAADF) scanning transmission electron microscopy (STEM) images using an image-based strain analysis method [13]. The lattice strain can also be directly measured using diffraction [14]. Direct imaging based on the scattering intensity distribution is a third possible approach: Caspary [15] reported, for example, the determination of a N content of 2.5–3% in a 186 nm thick, nearly uniform GaN_xAs_{1-x} layer by evaluating the contrast of annular dark field (ADF) images taken at different collection angle intervals. The nature of the N incorporation has also been reported. Tang and coworkers found that the incorporated N in dilute-nitride GaN_xAs_{1-x} epilayers grown by molecular beam epitaxy (MBE) with $x = 0.01$ to 0.04 was primarily interstitial [16].

Here, we have determined the N content and the nature of N incorporation in the GaN_xAs_{1-x} films on GaAs (001) substrates grown by MBE using TEM, STEM and CBED. The GaN_xAs_{1-x} films gave different contrast than the GaAs buffer in both TEM and STEM images. However, neither the state-of-the-art STEM-EELS nor energy dispersive X-ray spectroscopy (EDS) were able to give definite signals from nitrogen in these films. To overcome these limits and develop a quantitative method, we applied the newly developed energy-filtered (EF) scanning convergent beam electron diffraction (SCBED) technique to the GaN_xAs_{1-x} thin film samples. The goal was to examine the structure factors and the lattice parameters, since both are dependent on the N concentration and the nature of N incorporation. Through the refinement of high quality CBED patterns acquired using EF-SCBED, we demonstrate that the GaN_xAs_{1-x} film composition can be determined experimentally from the measured structure factors and provide evidence of N substitution and As vacancies. Thus, this paper establishes SCBED as a technique for characterization of atomic composition in dilute-nitride GaN_xAs_{1-x} epilayers.

2. Materials and methods

Three GaN_xAs_{1-x} epilayers with different N content were grown on 500 μm thick GaAs (001) substrates using a Veeco GEN 930 MBE system equipped with a Veeco SUMO source for Ga, a Veeco Mark V valved cracker source for As_2 and a Veeco UNI-Bulb RF plasma source for nitrogen. GaN_xAs_{1-x} epilayers of 300-500 nm in thickness were grown at 460°C at the rate of 1 μm/h on a 200 nm thick GaAs buffer epilayer (Fig. 1a). The nitrogen concentration of the prepared samples was first determined by high-resolution X-ray diffraction (HRXRD) (see Fig. 1b for an example) using Vegard's law [17], which gave the estimated molar fractions (x) of 1.0%, 2.4% and 6.4% for the three studied epilayers. The HRXRD was performed using a Bruker D8 Discovery High-Resolution Diffractometer using Cu Kα radiation (1.5406 Å). For convenience, we will refer to the samples by the N percentage obtained from HRXRD for the subsequent discussions. The nominal thicknesses of the grown GaN_xAs_{1-x} films were 300 nm for the 1.0%N and 6.4%N samples, and 500 nm for the 2.4%N sample.

Cross-section TEM samples were prepared both by focused ion beam (FIB) and Ar^+ ion-milling. FIB samples were prepared using a FEI Helios G4 UX dual-beam FIB. Initial Ga^+ ion-beam thinning was done at 30 kV acceleration voltage followed by final thinning at 5 kV and 2 kV to minimize the surface damaged layer on either side of the lamellae. A PIPS II was used to thin the Ar^+ ion-milled samples. The acceleration voltage of the ion beam was initially set at 3.5 kV before gradually reduced to 0.2 kV in the final stages of the milling. The samples were cooled by liquid nitrogen during milling.

TEM characterization was performed on a double Cs aberration corrected JEOL ARM-200CF, with a cold field emission gun (FEG) operated at 200 kV. The microscope is equipped with a 100 mm^2 Centurio EDS detector (covering a solid angle of 0.98 sr) and a Quantum ER GIF for dual EELS. STEM images were acquired with a semi-convergence angle of 27 mrad. Both EDS and EELS data were collected with a 110 pA beam current. A 67 mrad semi-collection angle combined with 0.1 eV/channel dispersion, giving 0.7 eV energy resolution based on the full width half maximum of the zero-loss peak, were used in the presented EEL spectra.

SCBED was performed in the TEM mode. This technique is an extension of CBED. Using the TEM deflection coils, the probe is scanned and CBED patterns are recorded from an area of the sample for every probe position, to provide spatially resolved structural information [18]. The measured probe size is less than 2 nm. The energy-filtered CBED patterns were collected using a custom DigitalMicrograph™ script [19, 20]. The advantage of SCBED is that it acquires multiple diffraction patterns, from which the best patterns can be selected for quantitative analysis of local structures. The energy-filtering (necessary to remove the inelastic background intensities) was performed by placing an energy selecting slit of 10 eV around the zero-loss peak. The electron beam acceleration voltage was calibrated using an experimental pattern collected from the GaAs substrate as described below.

Quantitative structure factor measurements were done using the refinement method described by Zuo and Spence [21–27]. The independent atom model obtained using Doyle-Turner atomic scattering factors [28] were used as the starting points for the structure factor refinement. In addition to the structure factors, parameters for local

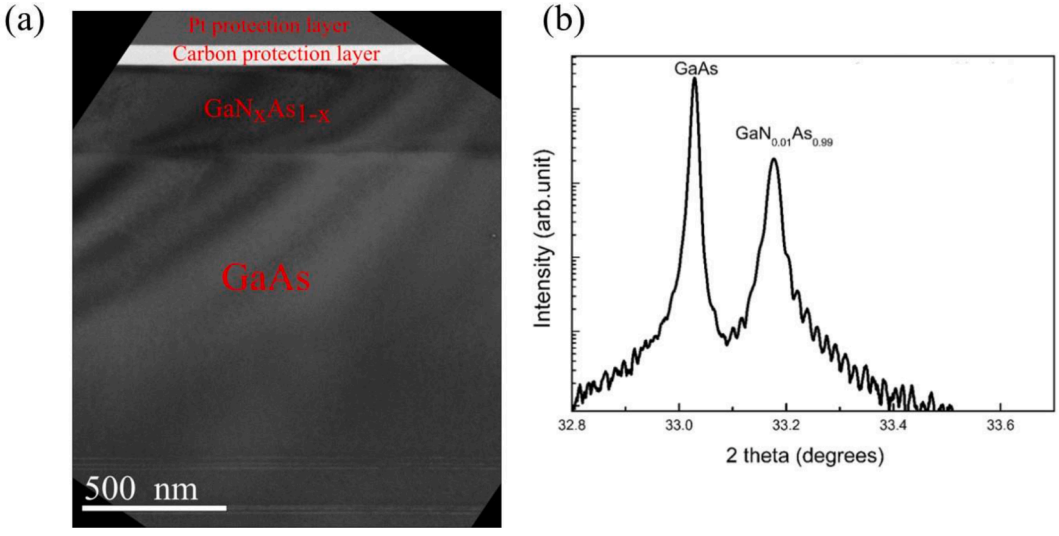

Fig. 1. Bright-field TEM image (a) and XRD spectrum (b) of GaN_xAs_{1-x} film grown on GaAs (001) substrate. A nitrogen molar fraction (x) of 1.0% is deduced from XRD based on Vegard's law.

sample thickness and diffraction geometry were also refined.

3. Results and discussion

3.1. Material quality

The quality of the MBE grown GaN_xAs_{1-x} epilayers was examined using both TEM and STEM imaging. Fig. 2 shows selected images obtained from the three different samples. The 6.4%N (Fig. 2a) and 1.0%N (Fig. 2b) samples, both with a film thickness of 300 nm, had uniform GaNAs epilayers without observable defects at this resolution, while the 500 nm thick film with the intermediate N concentration 2.4%N (Fig. 2c) was highly defective with misfit dislocations. This was also indicated by the broader peaks in the HRXRD patterns (not shown) from the 2.4%N sample. The misfit dislocations were introduced as a mechanism for strain relaxation. Such relaxations occur at a critical thickness, which we estimated to be between 300 and 500 nm for the 2.4%N GaNAs epilayers on GaAs.

Fig. 2d shows a higher resolution HAADF-STEM image of a misfit dislocation. The dumbbell structure of GaAs along the [110] projection is clearly resolved. A stacking fault is observed at the dislocation core and marked in the image. The dumbbells near the core show a complex contrast, which is not atomically resolved, in contrast to similar defects obtained in compound semiconductors [29]. The more complicated dislocation core contrast suggests a possible effect of the N atoms.

3.2. Evidence of change of lattice parameter in the GaNAs thin film

Selected area electron diffraction was employed to examine the difference in the lattice parameter between the GaNAs thin film and the GaAs buffer layer. Fig. 3 provides an example, where the diffraction pattern was recorded from the circled area in 3b covering both the GaAs buffer and the GaNAs thin film for the sample with 6.4%N. The thin film normal direction is [001]. Along this direction, a split in the (004) diffraction spot is observed, while no splitting is observed for (220). The size of the splitting corresponds to a 1.2% change in the c lattice parameter, which demonstrates that the GaNAs film has a tetragonal structure. The lattice parameter along the growth direction is reduced in the film compared to the GaAs buffer when As is substituted by the smaller N atom. From the split, we found that the film has a lattice parameter of 5.59 Å, as compared to 5.65 Å for the pure GaAs. According to Vegard's law, this indicates that the molar fraction x is around 0.03 (3%N) in the 6.4%N sample, which is about half of the molar fraction deduced from the XRD measurements. The difference between the TEM and XRD measurements comes from the combination of two factors. First, electron diffraction measures a small sample region (~200 nm), whereas the XRD was carried out over a ~mm range. Second, electron diffraction was performed on a thin cross-sectioned TEM lamella, while XRD was done on the as-grown sample. Thus, the lattice constants found from electron diffraction could also be impacted by the thin-film relaxation effect.

3.3. Evidence of compositional change in the GaNAs thin film

The (002) structure factor is sensitive to the composition, according to

$$F(002) = 4[f_{Ga} - (1-x)f_{As} - xf_N], \quad (1)$$

where $x = 0$ in the GaAs buffer layer. For $x \neq 0$, we assume a substitutional occupancy of N at the As sites.

Dark-field TEM imaging using the (002) reflection to form the image was done to check if this technique could image a compositional change between the GaAs buffer layer and the GaNAs thin film. Fig. 4 shows an example of a (002) dark field TEM image taken from the 1.0%N sample. The sample was tilted away from the [110] zone axis to the systematic row diffraction condition shown in Fig. 4a with the reflection (002) close

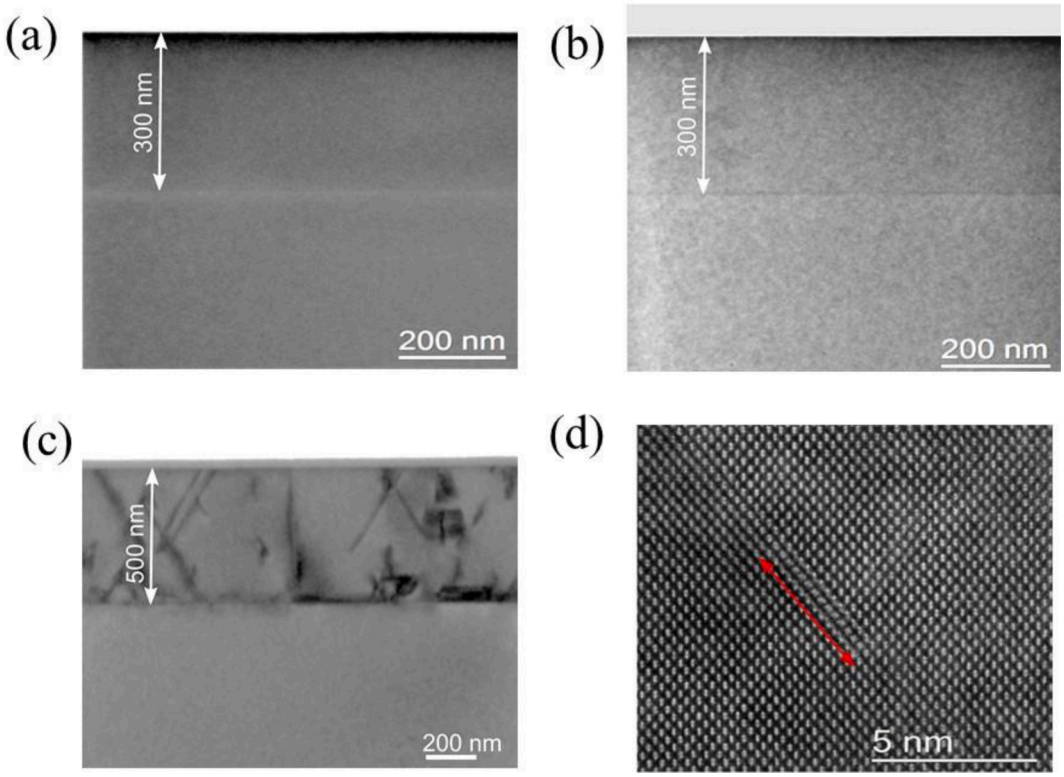

Fig. 2. Film quality of GaN_xAs_{1-x} films for different N compositions and film thicknesses. (a) 6.4% N /300 nm (b) 1.0%N /300 nm (c) 2.4%N /500 nm. The 500 nm film contains both stacking faults and dislocations. (d) Shows a high-resolution HAADF-STEM image from one of the stacking faults found near the interface in the 500 nm (2.4%N) thick film. The dislocation core is marked in the image.

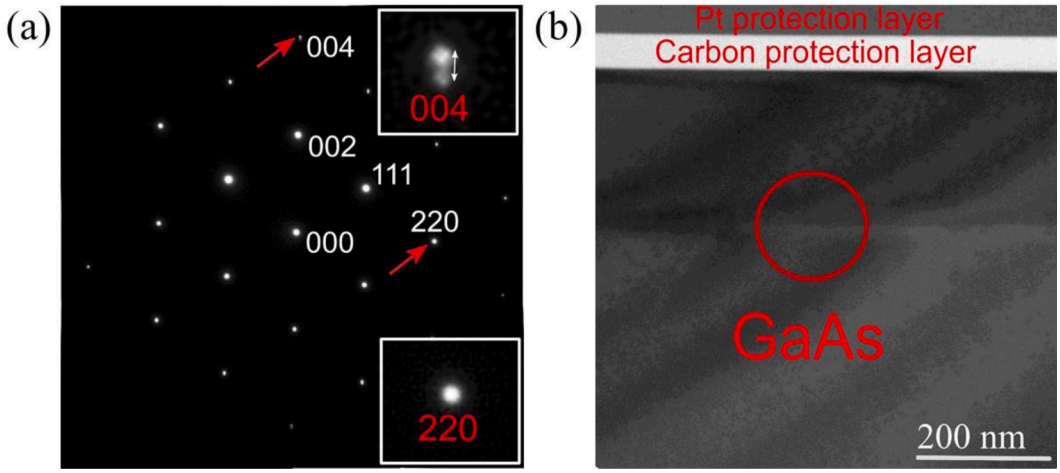

Fig. 3. Diffraction pattern (a) with corresponding BF-TEM image (b) taken from the interface between GaAs and GaN_xAs_{1-x} in the 6.4%N film. The SAED pattern is taken from an area covering the 300 nm in diameter circular region shown with a red circle in (b). The splitting is pointed out by the red arrow in (a) and corresponds to a 1.2% reduction in lattice parameter between substrate and film. The (004) and (220) reflections are pointed out by red arrows in (a) and shown in the insets. The splitting in (004) corresponds to a 1.2% reduction in lattice parameter between substrate and film. (For interpretation of the references to the color in this figure legend, the reader is reffered to the web version of this article.).

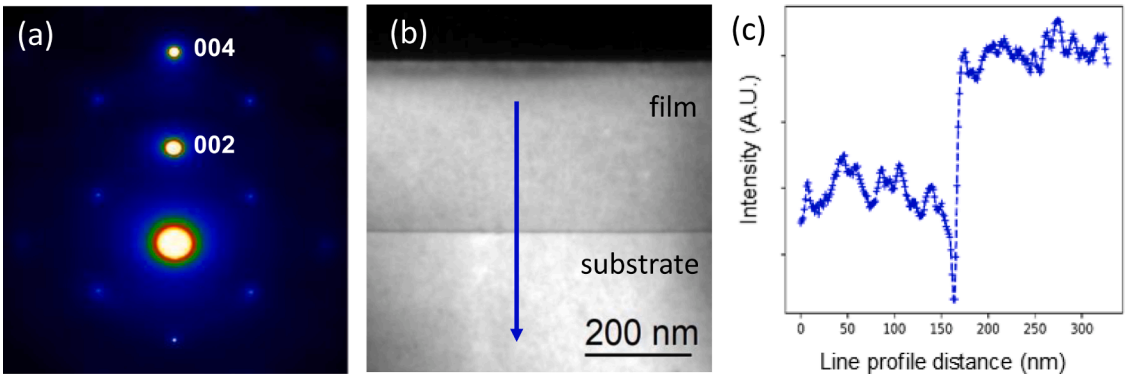

Fig. 4. (a) Selected-area diffraction pattern from the 1.0%N film, tilted ~10° from the [110] zone axis, in a diffraction condition close to the systematic row. (b) Corresponding dark field TEM image formed using the (002) reflection. (c) Intensity line profile along the blue arrow in (b). (For interpretation of the references to color in this figure legend, the reader is referred to the web version of this article.).

to the Bragg condition. A small objective aperture was placed on (002) to form the image in (b). The contrast of the GaNAs film is observably darker than the GaAs buffer. This is further demonstrated by the line profile in Fig. 4c. In GaAs, $|F(002)| = 4|f_{Ga} - f_{As}|$ which is reduced as the larger Z As atom is substituted by N (with a smaller atomic scattering factor). according to Eq. (1). The relatively uniform contrast in the low-resolution TEM image of Fig. 4 also suggests that the N distribution in the 1.0%N sample is relatively uniform at the tens of nm length scale. However, relating the TEM image contrast difference to the N amount in the film is difficult.

3.4. Compositional analysis of GaNAs thin films using STEM/EELS/EDX

STEM-EELS and EDS were performed to detect the presence of N in the GaN_xAs_{1-x} films. For this purpose, we selected the 6.4%N sample, which has the highest N concentration according to the XRD results. Fig. 5a and b show two ADF STEM images taken with semi-collection angles of 67 – 155 mrad and 155 – 470 mrad, respectively. The 300 nm thick 6.4%N GaNAs film displays higher contrast than the GaAs substrate in Fig. 5a due to strain. The strained film also gives diffuse scattering that contributes to the signal in this image. The HAADF STEM image (Fig. 5b) shows similar contrast for both the GaNAs film and the GaAs substrate.

EDS and EELS line scans were acquired across the GaAs buffer layer and the film. Each of the spectra in Fig. 5 is the sum of more than 100 spectra in the line scan. Neither in the EEL nor in the EDS spectrum can any significant signal from N, compatible with the nominal composition of $GaN_{0.064}As_{0.936}$, be detected. In the EEL spectrum the position of the N K-edge is expected at an energy loss of 401 eV (marked by a red line in Fig. 5c). In the EDS spectrum the N K-peak should appear at 0.39 keV, between the minor carbon contamination peak and the oxygen peak from surface oxidation. The inset shows that these signals are very small compared to the signals from Ga and As L-peaks. However, the Ga:As peak ratio differs significantly between the substrate and the film. This is shown in Fig. 5e, where the As K-peak in the film is significantly lower than that in the substrate after normalizing the spectra according to the Ga K-peak. The peak normalization was performed by making the integrated intensities under the Ga K-peak equal in the spectra from the buffer layer and the thin-film. After peak normalization, the As L-peak shows a similar decrease as the K-peak, when it is compared to the GaAs buffer layer (inset in Fig. 5d). Quantification of the Ga:As peak ratio in the 300 nm GaNAs film gives a chemical ratio of 51.2:48.8, i.e. a chemical composition of $GaN_{0.047}As_{0.953}$ under the assumption that the chemical composition is stoichiometric between III and V type of atoms (i.e. we assume that there are no interstitials or vacancies).

Thus, neither EDS nor EELS were able to give any clear signal from

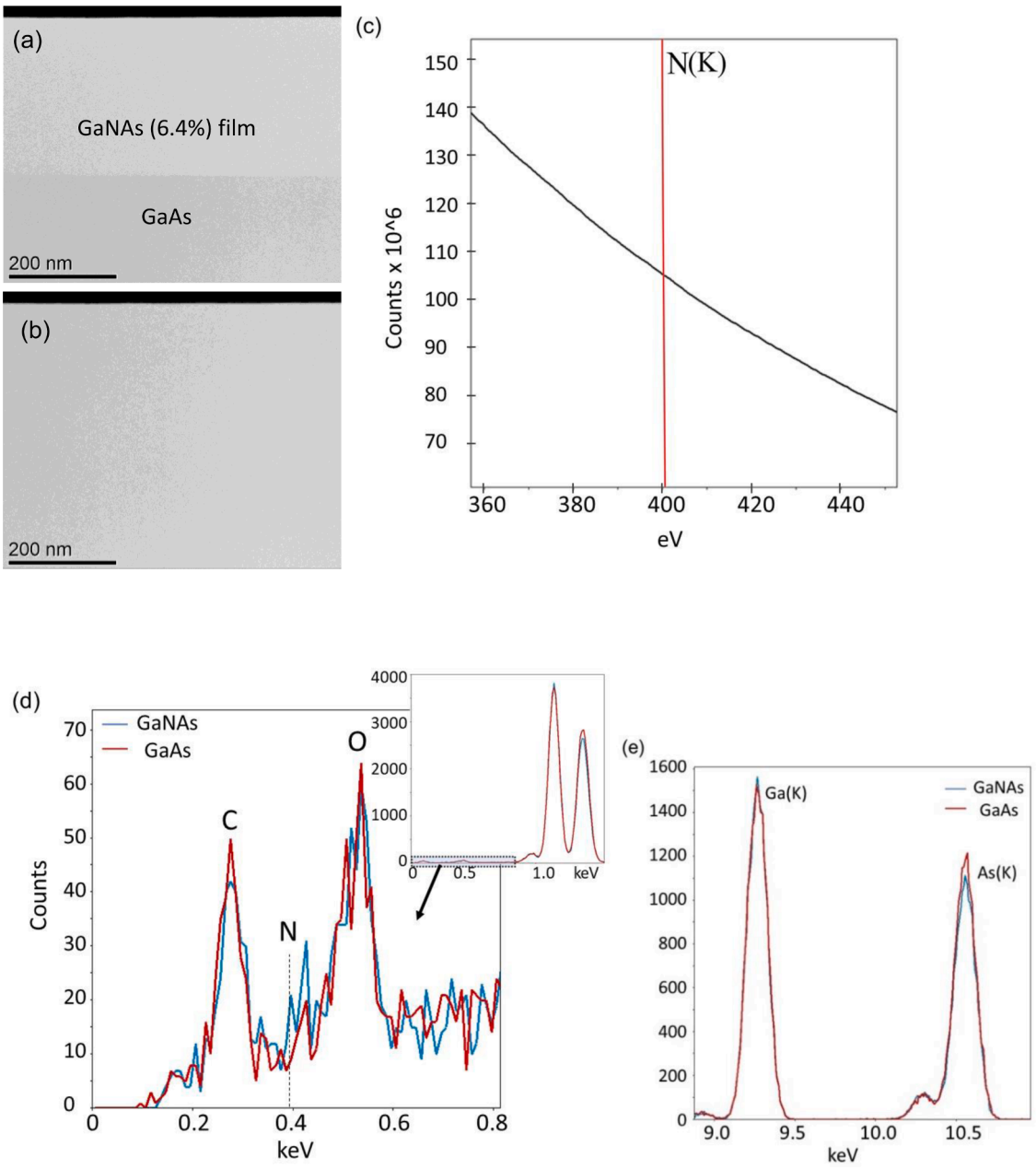

Fig. 5. Dark field STEM, EELS and EDS characterization of the 6.4%N sample. (a) ADF image recorded using semi collection angles between 67 and 155 mrad, (b) HAADF image using semi collection angles of 155-470 mrad. (c) and (d) are the averaged EELS and EDS spectra within the thin film. (e) Comparison between the average Ga and As K-peaks in the EDS spectrum.

nitrogen. As evidences of N are observed in both diffraction and dark field imaging experiments, the lack of signal can only be attributed to either the small inelastic scattering cross-section of N in the GaNAs films or the instability of N atoms under irradiation [30].

3.5. Refinement of N occupancy using quantitative scanning CBED

With EDS and EELS being insensitive to the nitrogen in the GaNAs samples, we turned to CBED to quantify the N concentration through structure factor refinements.

An accurate value of the electron acceleration voltage is needed for CBED refinement [31]. We therefore first performed pattern matching to determine the high voltage [32,33]. In this method the higher order Laue zone (HOLZ) patterns are filtered and matched with Bloch wave simulations to avoid errors due to dynamical effects. Fig. 6 shows the matching results for four different regions recorded using a large condenser aperture. The pattern was recorded from the GaAs buffer layer and the best match was obtained with a high voltage at 202.3±0.1 kV, using a fixed GaAs lattice parameter of a=5.653 Å. This high voltage was used in the rest of the CBED experiments.

Scanning CBED patterns were recorded using a 2D digital detector, in this case a CCD camera. Compared to CBED, which records one diffraction pattern for one probe position, SCBED collects the full 4-D data, in the form of two spatial coordinates, the (x, y) in the real space and the (k_x, k_y) in the reciprocal space. SCBED differs from scanning electron nano-diffraction (SEND) [18,34] by the beam convergence angle, which is larger for SCBED.

Fig. 7 shows an example of a SCBED experiment for the 6.4%N sample. The CBED patterns were acquired from a rectangular sample region of 30×300 nm^2 across the GaNAs film in a 10×100 pixel scan with a step size of 3 nm. Fig. 7a–c show the virtual BF, DF (002), and DF (004) images [35], reconstructed from the SCBED dataset across the

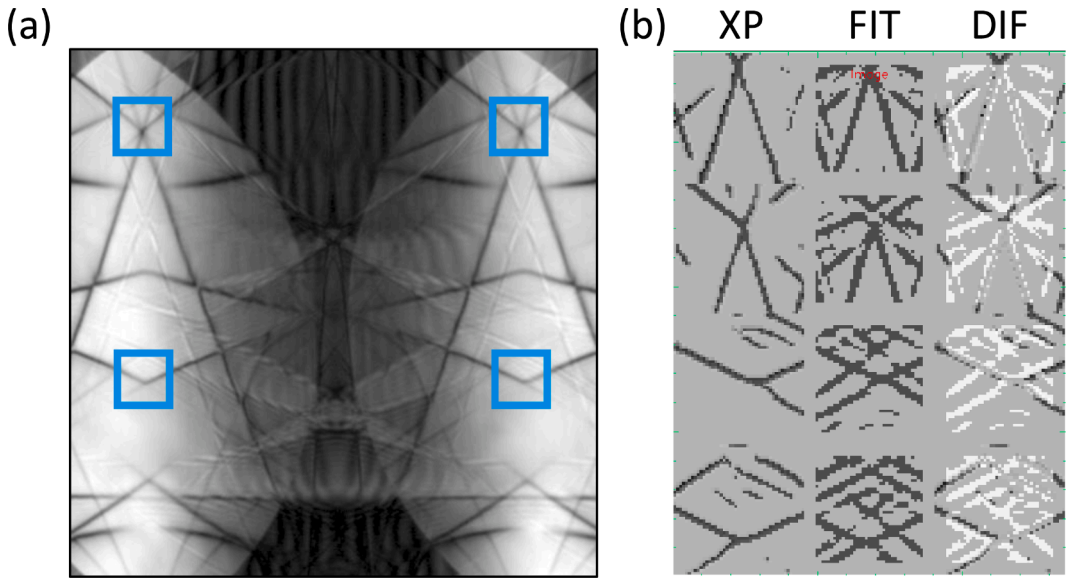

Fig. 6. TEM high voltage calibration using QCBED. (a) An experimental energy-filtered CBED pattern of GaAs near the [220] zone axis. The blue boxes are regions marked for refinement. (b) High voltage refinement results by comparing the experimental HOLZ lines (XP), calculated HOLZ lines (FIT), and their difference image (DIF). The high voltage was determined as 202.3±0.1 kV. (For interpretation of the references to color in this figure legend, the reader is referred to the web version of this article.).

entire GaNAs film. The SCBED dataset was analyzed using correlation grouping, where patterns with high correlation coefficients are grouped together and averaged [18]. Fig. 7b shows one selected experimental CBED pattern averaged from region B in (a). As explained in the method session, the patterns were energy-filtered using the GIF setup.

The quality of the CBED patterns indicates good crystallinity of the film, but the HOLZ lines, which appear in the simulated patterns, are not observed in the experimental patterns, indicating a large static Debye-Waller factor in the N-containing film [36,37]. From the SCBED dataset acquired across the film, we also noticed a change in the rocking curve fringes in the (004) disk, as well as inhomogeneous intensity variations in the (002). These features indicate a gradual thickness change of the TEM specimen and possibly local inhomogeneities in N concentration, respectively. The intensity variations of the (002) disk can also be seen from the DF (002) image reconstructed from SCBED dataset (Fig. 7a).

The information provided by CBED is the intensity versus S_g (deviation from the Bragg condition), or rocking curve information, which can be used for quantitative structure factor measurements [21–27]. CBED is known for its accuracy for structure factor determination, however, most CBED work has been carried out on bulk crystals where inhomogeneities are small or negligible. The SCBED method allows us to acquire high quality CBED patterns from relatively inhomogeneous materials, such as thin films.

To see if the relative amount of N can be directly determined from the CBED intensities, we performed quantitative CBED pattern refinement on data from the GaNAs films. N partial occupancy was the only structural parameter that was fitted, the other parameters used in the fitting were the local sample thickness and the diffraction geometry. The electron high voltage was set to the calibrated value of 202.34 kV. The refinement assumes a total occupancy of 1 for Ga at the anion site and N substitution for As.

We note that the largest discrepancy between experimental and simulated CBED patterns are caused by the geometric distortions, which come from the image corrector and the post-column GIF. To circumvent this, we took intensity line profiles for QCBED fitting mostly along the systematic row direction. The second discrepancy is the weaker contrast of deficient HOLZ lines in the experimental (002) disk, as discussed before. We circumvented this by taking line profiles in the (002) disk from regions away from the HOLZ lines.

Fig. 7c and d show the refinement result for the 6.4%N sample. Fig. 7c had the best match with the experimental pattern in Fig. 7b and gave a N concentration of 4.7%. We also fitted other CBED patterns in the SCBED dataset separately, and the QCBED fitting results gave nitrogen concentrations that varied between ~2 and 6%, with an average value of ~3.5%. Thus, the SCBED measurements of the 6.4%N indicated a N concentration lower than the value obtained from HRXRD.

3.6. *Refinement of the (002) structure factor in GaNAs*

The CBED refinements described in the previous section assumed a full occupancy for the anion site (e.g., the composition of the thin film is GaN_xAs_{1-x}). However, in real films, there is a possibility of vacancies at the As sites as a result of the N incorporation. To check for this possibility, we refined the (002) structure factors directly from the acquired CBED patterns. For this purpose, we selected the 1.0%N sample, which is of high structural quality. We included both (002) and (004) structure factors in the refinement, since the $F(002)$ is the most sensitive to N concentration changes according to Eq. (1), while the $F(004)$ is relatively insensitive to small changes in N composition according to

$$F(004) = 4[f_{Ga} + (1-y)f_{As} + xf_N] \quad (2)$$

where y is equal to x plus the As vacancy percentage, (1-y) specifies the As composition and x corresponds to the N substitution on As sites. When x=y there are no vacancies. Because of this, the (004) CBED disk can be used to determine the sample thickness as well, which is required to quantify the (002) disk diffraction intensity and the measurement of F(002).

Fig. 8 shows the QCBED analysis of the 1.0%N film for structure factor refinement. Fig. 8a is an experimental CBED pattern from the SCBED dataset acquired at an orientation of ~5° tilted away from the [110] zone axis. To refine this pattern, we first assumed a tetragonal distortion along the c-axis, then the lattice parameters (a, c) were refined based on the HOLZ lines recorded in the (000) disk using the same method that was used for high voltage determination. The lattice parameter refinement gave a=5.6537 Å and c=5.6475 Å, corresponding to a 0.11% tetragonal strain.

The electron structure factors $U(002)$ and $U(004)$ were refined next

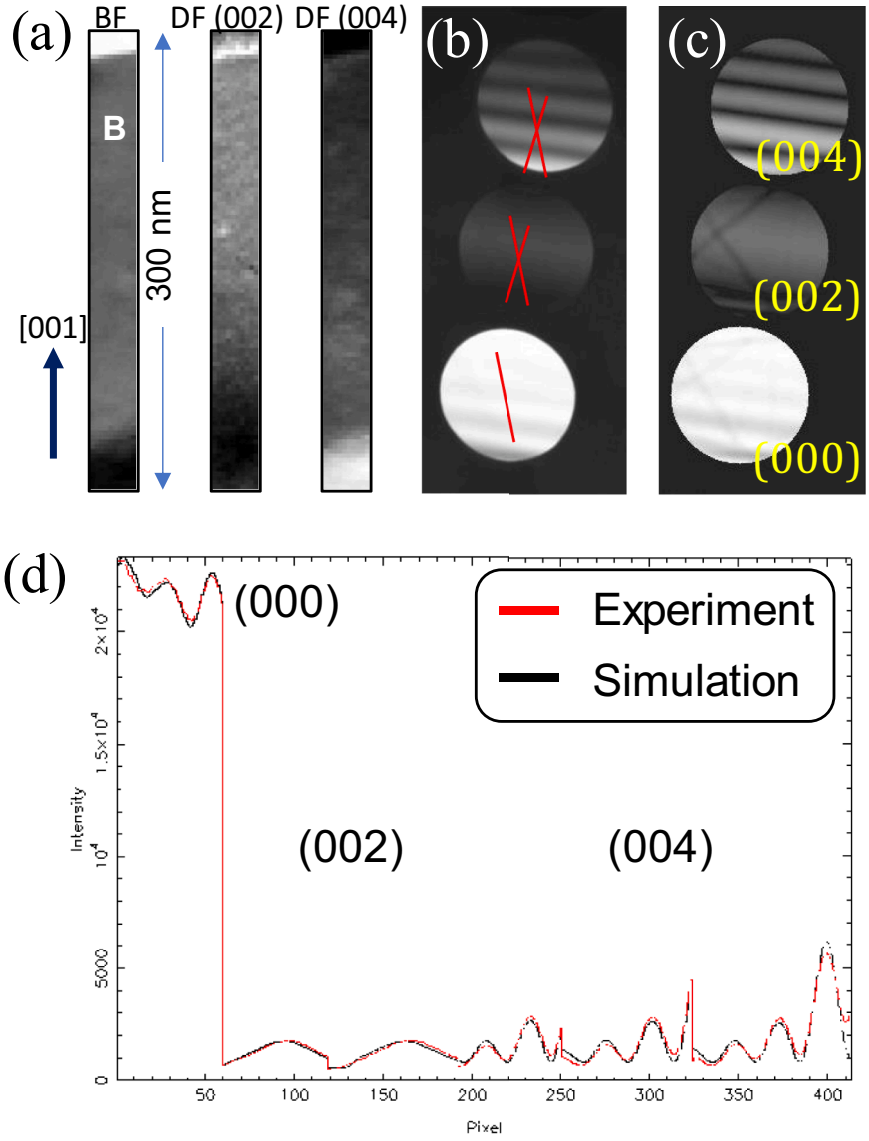

Fig. 7. CBED intensity refinement for the 6.4%N sample. (a) Virtual BF, DF (002), and DF (004) reconstructed from the SCBED dataset across the entire GaNAs film, with a scanned area of 30×300 nm^2. (b) The selected experimental CBED pattern from region B in (a), (c) Corresponding simulated CBED pattern after refinement. (d) The intensity line profile of the simulated (black) with the experimental (red) line profiles taken from (b). (For interpretation of the references to color in this figure legend, the reader is referred to the web version of this article.).

by comparing intensities along the marked red lines in Fig. 8a. The best fitting result is shown in Fig. 8c, where the experimental intensity is plotted in red and the fitted intensity in black. We then repeated the measurement at 10 different electron probe positions. The obtained refinement results for $U(002)$ are listed in Table 1 together with the conversion to the X-ray structure factor $F(002)$ and the calculated $F(002)$ using the following partial occupancy model

$$F(002) = 4[f_{Ga} - (1-y)f_{As} - xf_N] \quad (3)$$

where we have considered two models, i) $y = x$ assumes that N is purely substitutional into As sites while ii) $y = x+0.01$, accounts for 1% As vacancies. The Doyle-Turner atomic scattering factors were assumed in the calculations [28]. The bonding effect lowers the $F(002)$ value of GaAs by 5% according to Zuo et al. [24]. The average value of $F(002)$ from CBED refinement of the GaNAs is 3.22 e per unit cell, compared to the $F(002)$ value of 5.4 e per unit cell for GaAs. The effect of tetragonal distortion changes $F(002)$ by ~0.03 e per unit cell, which is even smaller. Thus, chemical composition is the dominant factor here.

From Table 1 the average N occupancy is 2.5% if we assume the full occupancy model ($y = x$, with x averaged to 0.025). This is unrealistic, since the N concentration as deduced from HRXRD is only 1.0%. From our measurement of N occupancy in the 6.4%N sample presented above, the actual occupancy is lower than the value deduced from HRXRD. The amount of N measured at ~3.5% in the 6.4%N sample is also lower than the 4.7%N estimated from the QCBED analysis using the full occupancy model.

The discrepancy here suggests the presence of As vacancies. To check for this possibility, we calculated $F(002)$ with the N occupancy of $x = 0.01$. To match the $F(002)$ obtained from QCBED, 1% As vacancies is then required, i.e. $y = 0.02$. The structure factor $F(002)$ is more sensitive to As vacancies than N occupancy, because of the larger atomic scattering factor of As compared to that of N. Thus, a small variation in N content will not significantly change the estimate of As vacancies.

The fluctuations in the $F(002)$ values obtained at different locations in the thin film are relatively small with a variance of 0.04 or sigma = 0.2, which is less than 10% of the measured $F(002)$ values. These fluctuations also include measurement errors due to film inhomogeneities, which impact the quality of the CBED patterns and thus the refinement results. Nonetheless, the small variance indicates that this effect is small. Thus, the results here represent a direct evidence of N occupancy and of N induced As vacancies in the GaNAs thin film.

The above results suggest a significant amount of As vacancies in the GaNAs thin films. The impact of such disorder in the as-grown material

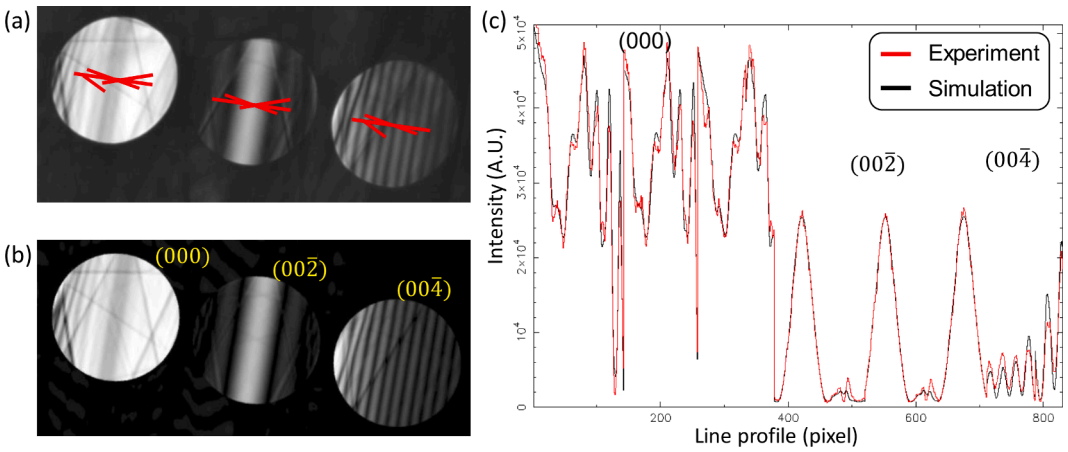

Fig. 8. CBED structure factor refinement for the 1.0%N sample. (a) An experimental energy-filtered CBED pattern acquired at an orientation of ~5° tilt away from the [110] zone axis, and (b) the corresponding simulated pattern after refinement. First, assuming a tetragonal distortion along the c-axis, the lattice parameters (a,c) were refined using the HOLZ lines as a=5.6537 Å and c=5.64745 Å, corresponding to 0.11% strain. The structure factors of $U(00\bar{2})$ and $U(00\bar{4})$were then refined, and the intensity fitting result shown in (c). The red lines in (a) indicate the intensity line profiles used for QCBED fitting. The red and black curves correspond to intensity line profiles of the experimental and refined simulated line profiles, respectively. (For interpretation of the references to color in this figure legend, the reader is referred to the web version of this article.).

Table 1
List of the N content and the $(00\bar{2})$ structure factors (U^e for electrons and F^x for X-rays). The electron and X-ray structure factors can be converted using the Mott formula. For retrieving the nitrogen occupancies, a tetragonal cell and two models were used. The first model assumes the pure substitution of N at As sites, i.e., the occupancies $occ_N + occ_{As} = 1$. The second model allows for some vacancies where occupancies $occ_N + occ_{As} < 1$. The right two columns list an example having 1% vacancies.

QCBED runs	U_002^e (Å^{-2})	R-factor	N% (substitutional)	F_002^X (electrons per unit cell)	N% (1% vacancy)	F_002^X (electrons per unit cell)
Cubic GaAs	0.4438E-02	–	–	5.416	–	–
Tetragonal GaAs	0.4385E-02	–	–	5.384		
Tetragonal Ga0.98%NAs						
1	3.74000E-03	8.80	2.40	3.32	0.95	3.52
2	3.71000E-03	6.80	2.50	3.22	1.10	3.42
3	3.73000E-03	8.80	2.40	3.303	0.97	3.502
4	3.56700E-03	6.90	3.00	2.788	1.60	2.987
5	3.64300E-03	6.50	2.80	3.024	1.30	3.223
6	3.69200E-03	6.80	2.60	3.178	1.10	3.378
7	3.67700E-03	6.80	2.60	3.132	1.10	3.331
8	3.75100E-03	5.70	2.40	3.363	0.90	3.562
9	3.80400E-03	6.10	2.20	3.527	0.71	3.726
10	3.76600E-03	5.0	2.30	3.409	0.85	3.608
Average	3,708E-03 +-6,4237E-05	6.80	2.50	3.227	1.10	3,4+-0,2

on electron beam radiation effects is in general not well studied. There are two possible outcomes of the As vacancies. Firstly, the impurity-vacancy defect complex modifies the bonding energy of N and thus impacts on the knock-on damage threshold [38]. Secondly, As vacancies can act as traps for displaced N atoms. The lack of STEM-EELS and STEM-EDX signals, which typically are performed at a relatively high electron dose, and the stability of the sample under the lower dose conditions for electron imaging and diffraction, suggest that both factors are in play for GaNAs.

4. Conclusions

In summary, we have presented STEM-EELS/EDS and SCBED results from different GaN_xAs_{1-x} films to determine the N concentration in these films. Both in TEM and in STEM, the films gave different contrast than the pure GaAs buffer. However, neither EDS nor EELS were able to give any signal from nitrogen, in conflict with the fact that HRXRD indicated the presence of N. The average Ga and As L- and K-peaks in the EDS spectrum from the substrate and the film clearly showed that the relative amount of As compared to Ga was less in the GaNAs film than in the GaAs substrate. In contrast to the lack of N signal in EELS and EDS from the GaNAs films, CBED refinements of the *F*(002) structure factor gave direct evidence of N occupancy and As vacancies. The measurements were enabled by the electron energy-filtered scanning CBED technique. Based on the CBED results, we attributed the missing N signals in EDS and EELS to the electron beam irradiation effect in the presence of As vacancies. Together, these results demonstrate a sensitive method for the determination of atomic composition in crystalline thin films based on quantitative electron diffraction.

Declaration of Competing Interest

The authors declare that they have no known competing financial interests or personal relationships that could have appeared to influence the work reported in this paper.

Acknowledgement

This work was supported by the Research Council of Norway (RCN) under contract 228956. JMZ wants to thank NTNU for support via the Lars Onsager Professorship. The TEM and CBED work was performed using the NORTEM infrastructure (RCN 197405) at the TEM Gemini Centre, Trondheim, Norway. Saroj Kumar is acknowledged for support with the HRXRD experiments.

References

[1] T. Mano, M. Jo, K. Mitsuishi, M. Elborg, Y. Sugimoto, T. Noda, Y. Sakuma, K. Sakoda, Fabrication of GaNAs/AlGaAs heterostructures with large band offset using periodic growth interruption, Appl. Phys. Express 4 (2011), 125001.

[2] P. Krispin, S.G. Spruytte, J.S. Harris, K.H. Ploog, Admittance dispersion of n-type GaAs/Ga(As,N)/GaAs heterostructures grown by molecular beam epitaxy, J. Appl. Phys. 90 (2001) 2405.

[3] J.F. Geisz, D.J. Friedman, III–N–V semiconductors for solar photovoltaic applications, Semicond. Sci. Technol. 17 (2002) 769.

[4] S.R. Kurtz, A.A. Allerman, E.D. Jones, J.M. Gee, J.J. Banas, B.E. Hammons, InGaAsN solar cells with 1.0 eV band gap, lattice matched to GaAs, Appl. Phys. Lett. 74 (1999) 729.

[5] B. Sciana, I. Zborowska-Lindert, D. Pucicki, B. Boratynski, D. Radziewicz, M. Tlakzala, J. Serafinczuk, P. Poloczek, G. Sek, J. Misiewicz, Technology and characterisation of GaAsN/GaAs heterostructures for photodetector applications, OptoElectron. Rev. 16 (2008) 1.

[6] M. Kondow, K. Uomi, A. Niwa, T. Kitatani, S. Watahiki, Y. Yazawa, GaInNAs: a novel material for long-wavelength-range laser diodes with excellent high-temperature performance, Jpn. J. Appl. Phys. 35 (1996) 1273.

[7] W. Shan, W. Walukiewicz, J.W. Ager III, E.E. Haller, J.F. Geisz, D.J. Friedman, J. M. Olson, S.R. Kurtz, Effect of nitrogen on the band structure of GaInNAs alloys, J. Appl. Phys. 86 (1999) 2349.

[8] M. Fischer, D. Gollub, M. Reinhardt, M. Kamp, A. Forchel, GaInNAs for GaAs based lasers for the 1.3 to 1.5μm range, J. Cryst. Growth 251 (2003) 1.

[9] I.A. Buyanova, W.M. Chen, C.W. Tu, Defects in dilute nitrides, J. Phys. Condens. Matter 16 (2004) 3027.

[10] W. Li, M. Pessa, T. Ahlgren, J. Decker, Origin of improved luminescence efficiency after annealing of Ga(In)NAs materials grown by molecular-beam epitaxy, Appl. Phys. Lett. 79 (2001) 1094.

[11] A. Khan, J. Gou, M. Imazumi, M. Yamaguchi, Interaction of electron irradiation with nitrogen-related deep levels in InGaAsN, Appl. Phys. Lett. 90 (2007), 243509.

[12] M.K.H. Natusch, C.J. Humphreys, N. Menon, O.L. Krivanek, Experimental and theoretical study of the detection limits in electron energy-loss spectroscopy, Micron 30 (1999) 173.

[13] T. Grieb, K. Müller, R. Fritz, M. Schowalter, N. Neugebohrn, N. Knaub, K. Volz, A. Rosenauer, Determination of the chemical composition of GaNAs using STEM HAADF imaging and STEM strain state analysis, Ultramicroscopy 117 (2012) 15.

[14] R. Yuan, J. Zhang, J.M. Zuo, Lattice strain mapping using circular Hough transform for electron diffraction disk detection, Ultramicroscopy 207 (2019), 112837.

[15] K. Muller-Caspary, K. Oppermann, O. Grieb, et al., Materials characterization by angle-resolved scanning transmission electron microscopy, Sci. Rep. 6 (2016) 37146.

[16] D. Tang, G.K. Vijaya, A. Mehrotra, A. Freundlich, D.J. Smith, Investigation of dilute-nitride alloys of GaAsNx ($0.01 < x < 0.04$) grown by MBE on GaAs (001) substrates for photovoltaic solar cell devices, J. Vac. Sci. Technol. 34 (2016), 011210.

[17] L. Vegard, Die Konstitution der Mischkristalle und die Raumfüllung der Atome, Zeitschrift für Physik 5 (1921) 17.

[18] J.M. Zuo, Electron nanodiffraction, in: P.W. Hawkes, J.C.H. Spence (Eds.), Springer Handbook of Microscopy, Springer International Publishing Cham, 2019, p. 2.

[19] K.H. Kim, H. Xing, J.M. Zuo, P. Zhang, H.F. Wang, TEM based high resolution and low-dose scanning electron nanodiffraction technique for nanostructure imaging and analysis, Micron 71 (2015) 39.

[20] K.H. Kim, J.M. Zuo, Symmetry quantification and mapping using convergent beam electron diffraction, Ultramicroscopy 124 (2013) 71.

[21] J.M. Zuo, J.C.H. Spence, Automated structure factor refinement from convergent-beam patterns, Ultramicroscopy 35 (1991) 185.

[22] J.M. Zuo, M. Kim, R. Holmestad, A new approach to lattice parameter measurements using dynamic electron diffraction and pattern matching, J. Electron Microsc. 47 (1998) 121.

[23] K. Tsuda, M. Tanaka, Refinement of crystal structural parameters using two-dimensional energy-filtered CBED patterns, Acta Crystallogr. A 55 (1999) 939.

[24] J.C.H. Spence, J.M. Zuo, Electron Microdiffraction, Springer, Boston MA, 1992.

[25] J.M. Zuo, J.C.H. Spence, M. O'Keeffe, Bonding in GaAs, PRL 61 (1988) 353.

[26] B. Jiang, J.M. Zuo, J. Friis, J.C.H. Spence, On the consistency of QCBED structure factor measurements for TiO_2 (rutile), Microsc. Microanal. 9 (2003) 457.

[27] J.M. Zuo, Measurements of electron densities in solids: a real-space view of electronic structure and bonding in inorganic crystals, Rep. Prog. Phys. 67 (2004) 2053.

[28] P.A. Doyle, P.S. Turner, Relativistic Hartree-Fock X-ray and electron scattering factors, Acta Crystallogr. A 4 (1968) 390.

[29] D.J. Smith, Atomic-resolution structure imaging of defects and interfaces in compound semiconductors, Prog. Cryst. Growth Charact. Mater. 66 (2020), 100498.

[30] J.R. Srour, J.W. Palko, Displacement damage effects in irradiated semiconductor devices, IEEE Trans. Nucl. Sci. 60 (2013) 1740.

[31] R. Holmestad, C.R. Birkeland, K. Marthinsen, R. Høier, J.M. Zuo, Use of quantitative convergent-beam electron diffraction in materials science, Microsc. Res. Tech. 46 (1999) 130.

[32] J.M. Zuo, M. Kim, R. Holmestad, A new approach to lattice parameter measurements using dynamic electron diffraction and pattern matching, J. Electron Microsc. 47 (1998) 121.

[33] J.M. Zuo, Automated lattice parameter measurement from HOLZ lines and their use for the measurement of oxygen content in $YBa_2Cu_3O_{7-\delta}$ from nanometer-sized region, Ultramicroscopy 41 (1992) 211.

[34] J.M. Zuo, J. Tao, Scanning electron nanodiffraction and diffraction imaging, in: S. Pennycook, P. Nellist (Eds.), Scanning Transmission Electron Microscopy, Springer, New York, 2011.

[35] E.F. Rauch, M. Véron, Virtual dark-field images reconstructed from electron diffraction patterns, Eur. Phys. J. Appl. Phys. 66 (2014) 10701.

[36] F. Houdellier, C. Roucau, L. Clément, J.L. Rouvière, M.J. Casanove, Quantitative analysis of HOLZ line splitting in CBED patterns of epitaxially strained layers, Ultramicroscopy 106 (2006) 951.

[37] Y. Martin, J.L. Rouvière, J.M. Zuo, V. Favre-Nicolin, Towards a full retrieval of the deformation tensor F using convergent beam electron diffraction, Ultramicroscopy 160 (2016) 64.

[38] R.F. Egerton, P. Li, M. Malac, Radiation damage in the TEM and SEM, Micron 35 (2004) 399.